

# The Critical Influence of Spin-Dry Technique on the Surface Passivation Quality of Crystalline Silicon Solar Cell Structures

Vibhor Kumar, Munan Gao, and Ngwe Zin\*

This study examines the effects of spin-dry (SD) and N<sub>2</sub> blow-dry (ND) techniques on the quality and surface passivation performance of silicon oxide grown in ozone-dissolved deionized water. The SD method achieves greater oxide thickness uniformity, averaging 1.39 nm ± 4.17% across 49 points, compared to 1.68 nm ± 21.67% for the ND wafers. However, persistently poor passivation of ozonated oxide-grown wafers following the SD process is exhibited, with carrier lifetime,  $\tau_{\text{eff}} < 0.3$  ms and saturation current density,  $J_0$  (per side) ranging from 26 to 45 fA cm<sup>2</sup>. These findings are analyzed in the context of the fundamental phenomena involved in the drying processes of both techniques. Following this, an optimized spin-drying process is developed, resulting in improved  $\tau_{\text{eff}}$  and  $J_0$  values of 1.4 ms and 5.6 fA cm<sup>−2</sup>, respectively. Scanning electron microscopy further confirms that the oxide films dried with the enhanced SD technique are free of pinholes.

cell architectures like metal insulated semiconductor (MIS), polycrystalline silicon on oxide (POLO), and tunnel oxide passivated contact (TOPCon), SiO<sub>x</sub> serves as a thin-film dielectric layer. It prevents direct metal contact with the silicon surface, thereby reducing contact/interface recombination.<sup>[2–4]</sup> 3) Passivated contacts: SiO<sub>x</sub> plays a crucial role in the aluminum oxide-based passivation of *p*-type silicon surfaces in PERC cells. This implementation, known as “passivated contacts,” not only passivates the silicon surface but also enables tunneling carriers to reach the contacts.<sup>[5,6]</sup> These multifaceted benefits of SiO<sub>x</sub> make it a focal point of extensive research in PV technologies.

## 1. Introduction

Silicon oxide (SiO<sub>x</sub>) is a fundamental material in the silicon-based photovoltaic (PV) industry, demonstrating considerable versatility in the development of high-efficiency solar cells. Its applications include: 1) surface passivation: SiO<sub>x</sub> is employed to reduce interface state density by passivating dangling bonds on bare silicon wafers. This “surface passivation” is critical in cell technologies such as passivated emitter and local back diffusion (PERL), passivated emitter rear totally diffused (PERT), and passivated emitter and rear contact (PERC), where it precedes silicon nitride (SiN<sub>x</sub>) deposition.<sup>[1,2]</sup> 2) Dielectric layer: in various

The most common and industrially feasible method for growing SiO<sub>x</sub> is using a thermal furnace. However, high temperatures required can significantly impact the longevity of bulk carriers used in silicon wafers and contact metals. Additionally, a single thermal SiO<sub>x</sub> run can be time-consuming, often taking several hours to complete. These challenges highlight the need for low-temperature techniques for SiO<sub>x</sub> growth or deposition.<sup>[7,8]</sup> One such technique is plasma-enhanced chemical vapor deposition, which allows for SiO<sub>x</sub> deposition but is limited to single-side application per run, necessitating an extra processing step to deposit oxide on the other side of the wafer.<sup>[9]</sup> Another established method is nitric acid oxidation of silicon (NAOS). Although effective, NAOS involves high-temperature annealing (≈1100 °C) after oxide growth and uses hazardous chemicals, which limits its use in the development of PV devices.<sup>[10,11]</sup> Oxide grown by UV–ozone was also investigated by a number of groups,<sup>[12,13]</sup> but lowthroughput associated with the UV–ozone technique has hindered its viability in the development of silicon solar cells. Recently, ozone-dissolved deionized water (DI–O<sub>3</sub>) has emerged as a promising method for growing SiO<sub>x</sub> due to its cost-effectiveness, recyclability, safety, high throughput, and the ability to operate at room temperature. Despite previous studies evaluating its uniformity, quality, inline integration, and potential in modern cell architectures,<sup>[14–18]</sup> DI–O<sub>3</sub> is still in the early stages of adaptation within the PV industry. DI–O<sub>3</sub> oxide growth is a wet chemical process that involves multiple steps, including deionized water rinsing and drying. The oxide growth will initially be dependent on concentration of ozone in solution, followed by surface electric field-induced diffusion of O<sup>−</sup> anions that formed during dissociation of ozone at SiO<sub>2</sub>/liquid interface.<sup>[19]</sup> The wafer drying step is crucial, as it is the final stage before further processing. Contaminants or defects

V. Kumar


Rutgers University, now with Texas A&M University  
400 Bizzell Street, College Station, TX 77843, USA

M. Gao

Rutgers University, now with Canadian Solar Inc.  
545 Speedvale Avenue West, Guelph, ON N1K 1E6, Canada

N. Zin

Rutgers University: Rutgers The State University of New Jersey  
500 Bartholomew Road, Piscataway, NJ 08840, USA  
E-mail: ngwe.zin@rutgers.edu

 The ORCID identification number(s) for the author(s) of this article can be found under <https://doi.org/10.1002/pssr.202400314>.

© 2024 The Author(s). physica status solidi (RRL) Rapid Research Letters published by Wiley-VCH GmbH. This is an open access article under the terms of the Creative Commons Attribution License, which permits use, distribution and reproduction in any medium, provided the original work is properly cited.

DOI: 10.1002/pssr.202400314

introduced during this phase can negatively impact subsequent processes,<sup>[20]</sup> potentially affecting PV device performance. Common drying techniques include spin-dry (SD) and nitrogen blow-dry (ND). SD uses centrifugal force to remove water from the wafer, while ND involves blowing nitrogen gas to remove residual water.<sup>[21]</sup> Since these techniques operate on different principles, they have distinct effects on the wafer surface.<sup>[22]</sup> Key questions to address are: 1) how do different drying techniques impact the quality of DI-O<sub>3</sub> oxide? and 2) which technique yields better oxide quality and surface passivation? Here, oxide quality encompasses thickness uniformity and the presence of pinholes. Uniform thickness is crucial, particularly in MIS solar cells, where thinner oxide regions can cause leakage currents that reduce open-circuit voltage and overall cell efficiency. Thinner oxide layers may also result in higher interface state density, while thicker layers could improve open-circuit voltage but potentially degrade fill-factor and short-circuit current density.<sup>[23,24]</sup> In passivated contact cells, thinner oxide layers may offer poorer chemical passivation, while thicker layers can reduce field-effect passivation, block tunneling, and increase sheet resistivity.<sup>[25]</sup> Pinholes in PERC cells can create local recombination centers, increasing effective recombination velocity,<sup>[26,27]</sup> and in BC-BJ cell designs, pinholes can lead to local shunting and performance degradation.<sup>[28]</sup>

This work aims to address the key questions related to the integration of DI-O<sub>3</sub> oxide in the PV industry. It examines the commonly used wafer drying techniques—SD and ND—to evaluate their impact on DI-O<sub>3</sub> oxide. The study investigates critical parameters such as thickness uniformity, pinholes, and surface passivation quality for both SD and ND methods. Additionally, this work introduces an enhanced spin-drying process specifically designed for wafers treated with the DI-O<sub>3</sub> method. While this improved SD process is tailored for DI-O<sub>3</sub>, it also has broader applicability for other wet chemical oxide growth techniques.

## 2. Results and Discussion

First, n-type Cz wafers described in the experimental section went through the silicon etch in TMAH, surface-cleaned in DI-O<sub>3</sub> bath, grown with  $\approx 1.5$  nm of DI-O<sub>3</sub> oxide and DI water (DIW) rinse. Wafers were then split into two groups: one processed with ND and the other with SD. The oxide thickness uniformity and passivation quality of samples dried using SD and ND methods are shown in **Figure 1a,b**. The colormap of the grown SiO<sub>x</sub> dried using SD technique clearly reveals a lesser variation in the color (**Figure 1a**) compared to ND technique (**Figure 1b**). The uniformity in the oxide thickness was determined using ellipsometry, averaged over 49 points, resulting in  $1.39 \text{ nm} \pm 4.17\%$  for SD and  $1.68 \text{ nm} \pm 21.67\%$  for ND. In SD techniques, water droplets from rinsing are swept uniformly in all directions and quickly from the surface of silicon wafer by centrifugal force generated by spinning. However, in the case of ND, the sweeping of water from the wafer surface takes place from one region to another at a slower rate than SD case. Above facts pointed that huge variation in the thickness uniformity is due to relatively slow and uncontrollable drying process in ND case. Further, the effect of both drying techniques on surface

passivation is accessed by growing  $\approx 15$  nm AlO<sub>x</sub> using ALD followed by annealing at 450 °C for 30 min in N<sub>2</sub> ambient. The results in **Figure 1c** show that samples processed by SD were resulted with drastically inferior passivation quality ( $< 0.3$  ms of  $\tau$  and  $> 25 \text{ fA cm}^{-2}$  of  $J_0$  per side) than that by ND samples ( $\approx 1.3$  ms of  $\tau$  and  $< 5 \text{ fA cm}^{-2}$  of  $J_0$ ). However, the good passivation quality by ND comes at the expense of bad uniformity.

To identify if rinsing samples in DIW has any role on passivation quality, a DIW rinse step was omitted for DI-O<sub>3</sub> grown samples processed by ND and SD. Samples were deposited with 15 nm of AlO<sub>x</sub> and then annealed at 450 °C in N<sub>2</sub> for 30 min, followed the measurement of  $\tau_{\text{eff}}$  and  $J_0$ . **Figure 2** shows that both ND- and SD-processed DI-O<sub>3</sub> grown samples without the rinse step were resulted with equally poor passivation results.  $\tau_{\text{eff}}$  and  $J_0$  results in **Figure 2** indicate that rinsing the samples in DIW is essential for good passivation, since earlier results of ND-processed samples that included DIW rinse achieved good passivation results (see **Figure 1**).

Next, we turned our attention to whether including SD in samples already processed by ND has any role in the passivation quality. The experiment was continued by adding SD step following the drying of DI-O<sub>3</sub> oxide samples by ND (i.e., TMAH, DI-O<sub>3</sub> growth, DIW rinse, ND, and then SD). **Table 1** illustrates that when SD was added to DI-O<sub>3</sub> oxide samples that have already been processed by ND, the samples depict poor  $\tau$  and  $J_0$ , although with good passivation quality prior to SD application. Results in **Table 1** further confirm that if drying DI-O<sub>3</sub> oxide samples with SD as a last step, poor passivation performance will be exhibited.

Our investigation then turned into the sequence of applying SD to DI-O<sub>3</sub> oxide samples. We devised a drying sequence for DI-O<sub>3</sub> oxide-grown samples, ensuring that SD is not the last step. The sequence follows as DI-O<sub>3</sub> grown samples going through SD process, followed by DIW rinse, and then by ND, and we name this sequence as an improved SD. PCD results in **Figure 3** highlight that samples processed through the improved SD result in a significantly improved passivation performance (i.e.,  $\tau > 1.4$  ms and  $J_0 < 6 \text{ fA cm}^{-2}$ ), and these results are on par with samples processed by ND only.

Moreover, the ellipsometry measurement reveals that improved SD method delivers DI-O<sub>3</sub> oxide with the good uniformity  $< \pm 4\%$ , as shown in the inset of **Figure 3**. Findings of the above experiment confirm that improved SD method not only provides the good uniformity, but also the superior passivation quality on DI-O<sub>3</sub> oxide-grown samples; however, the questions remain on why 1) the passivation quality recovers, while 2) achieving the good uniformity despite ending the drying process with ND as a last step, as initially we thought ND did not provide good uniformity. Achieving the good uniformity by the improved SD technique can be explained in terms of how long ozone remains available for reaction with the silicon. It is already shown in the earlier section that SD provides very good uniformity owing to its quick process and centrifugal force. In the improved SD process, as the oxide layer is already formed during SD process there are merely any ozone-reactive species left to react with silicon and form the oxide. Such nonavailability of ozone is due to the removal of dissolved ozone water during SD process and very low half-life (a few minutes at room temperature) of ozone itself. Therefore, processes following SD, i.e., DIW and ND, have no impact on the oxide uniformity in the improved SD process.

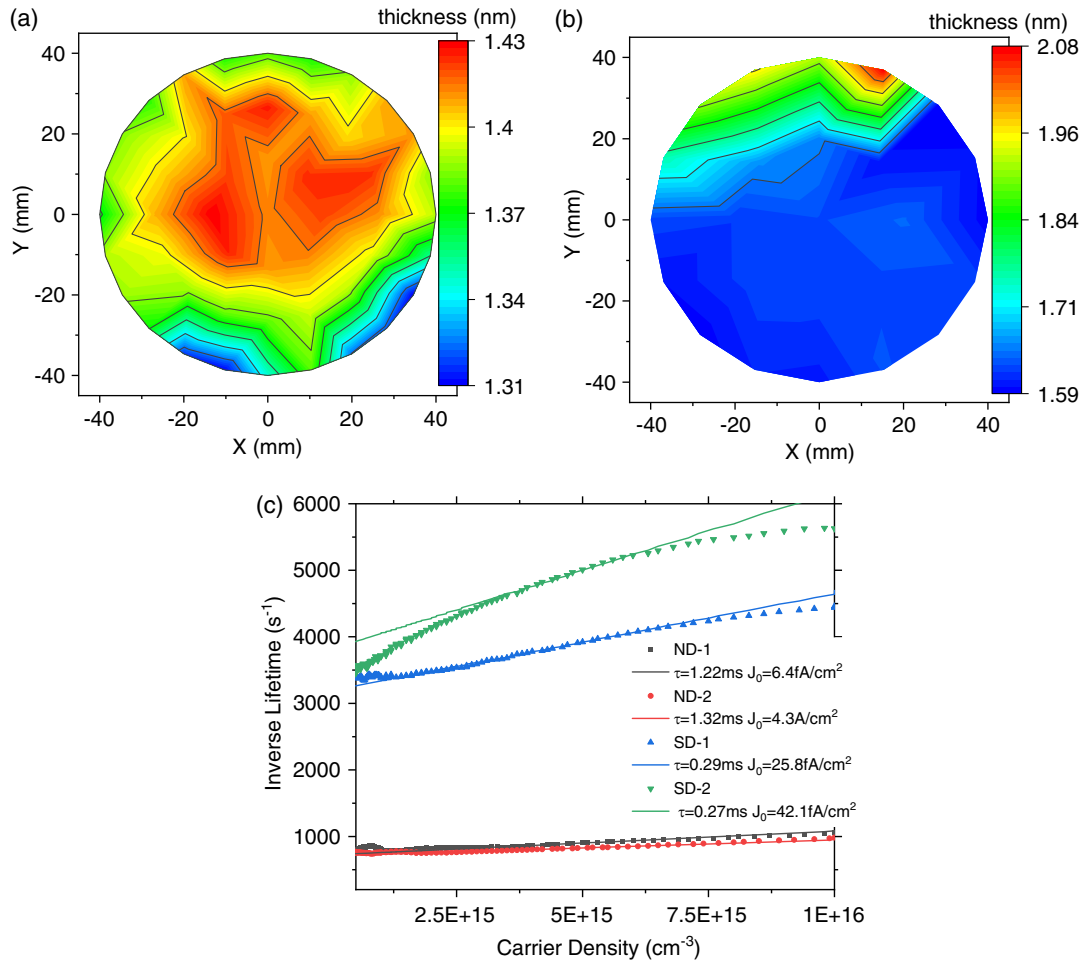


**Figure 1.** a) The thickness variation of DI-O<sub>3</sub> grown oxide layer with SD method, averaging thickness is 1.39 nm with uniformity of  $\pm 4.17\%$ . b) The thickness variation of DI-O<sub>3</sub> grown oxide layer with ND method, averaging thickness is 1.68 nm with uniformity of  $\pm 21.67\%$ . c) PCD measurement results of DI-O<sub>3</sub> grown oxide layer with both drying methods capped by ALD AlO<sub>x</sub>.

The recovery of poor passivation—induced as a result of drying DI-O<sub>3</sub> oxide samples by SD as a last step—by the improved SD technique is discussed in the following details. The passivation scheme employed in this contribution to prevent recombination of charge carriers at the surface of c-Si is based on the chemical passivation by DI-O<sub>3</sub> oxide<sup>[29]</sup> and field-effect passivation by fixed negative charges of AlO<sub>x</sub>.<sup>[30,31]</sup> Particularly, the field-effect passivation creates the electric field by fixed charge density at the interface that electrostatically shields one type of charge carriers to reach to the surface. Wafers processed by SD process after DI-O<sub>3</sub> oxide growth experiencing poor passivation could be

**Table 1.** PCD measurement results of DI-O<sub>3</sub> oxide samples ending with SD last and then capped by AlO<sub>x</sub>. NDthenSD #1 and #2 denote DI-O<sub>3</sub> grown samples are dried by ND, and then by SD.

Parameters	NDthenSD #1	NDthenSD #2
$\tau$ [ms]	0.25	0.24
$J_0$ [fA cm <sup>-2</sup> ]	27.9	24.7

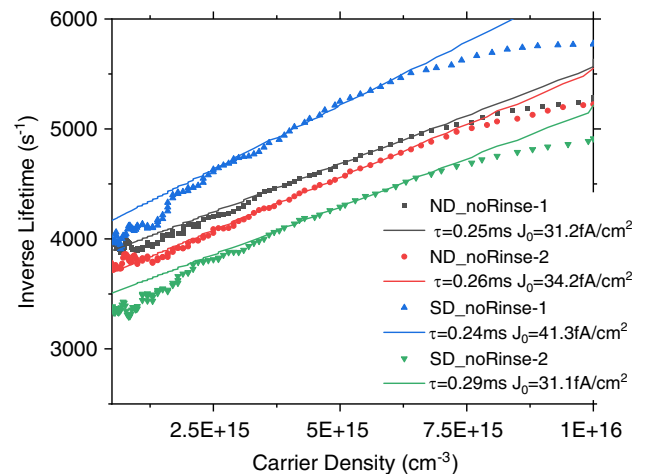


**Figure 2.** PCD measurement results of ND- and SD-processed DI-O<sub>3</sub> grown samples excluding the DIW rinse step, i.e., TMAH, DI-O<sub>3</sub> growth, and then ND or SD.

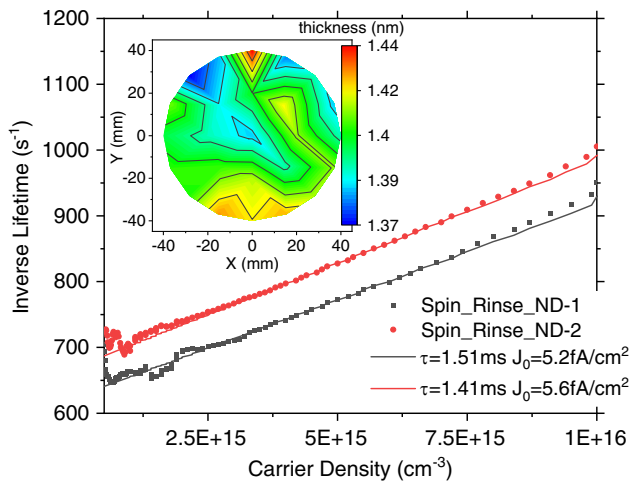


**Figure 3.** PCD measurement results of samples with DI- $\text{O}_3$  oxide processed by improved SD, then capped by  $\text{AlO}_x$ . Inset figure illustrates the uniformity of DI- $\text{O}_3$  oxide-grown sample processed by improved SD.

highly related to charges induced on the DI- $\text{O}_3$  oxide surface. Literature<sup>[32,33]</sup> revealed that in the course of drying wafer by SD process, the friction between the surface of the wafer and air induces static charges on the wafer surface, and the induced

charges do not dissipate itself from the wafer surface if any insulating layer is present on the surface of the wafer. Moreover, plastic cassettes to hold the wafers during the drying process could be additional source of static charges on the wafer.<sup>[34]</sup> The PCD measurements in this work and existing literature<sup>[33,35]</sup> revealed that there were excess of static positive charges induced on the surface of the oxide that deteriorate the passivation. This is because if negative charges were in excess, the passivation should be even better. An almost similar experiment has been reported in ref. [36], where on top of the  $\text{Al}_2\text{O}_3/\text{SiO}_2/\text{c-Si}$ , positive charges were induced using corona discharge method. It was found that when density of corona discharged positive charges is equal to the built-in negative charges in  $\text{AlO}_x$ , the lifetime of the sample was totally degraded. Considering above fact, SD-induced static positive surface charges will nullify the effect of the fixed negative present in  $\text{AlO}_x$  and which in turn deteriorates the passivation in the present work. Addressing on how poor passivation is recovered by improved SD technique, it is well known that deionized water contained some ionic impurities that may be attributed to piping, machinery, and static charges due to the charging of the DI water, etc.<sup>[37]</sup> When SD-processed samples were rinsed in DI water, the ionic impurities in DI water minimized/canceled the static charges present on the surface of the wafers. As a result, rinsing samples grown with DI- $\text{O}_3$  oxide and processed by SD in DI water revealed a good passivation.

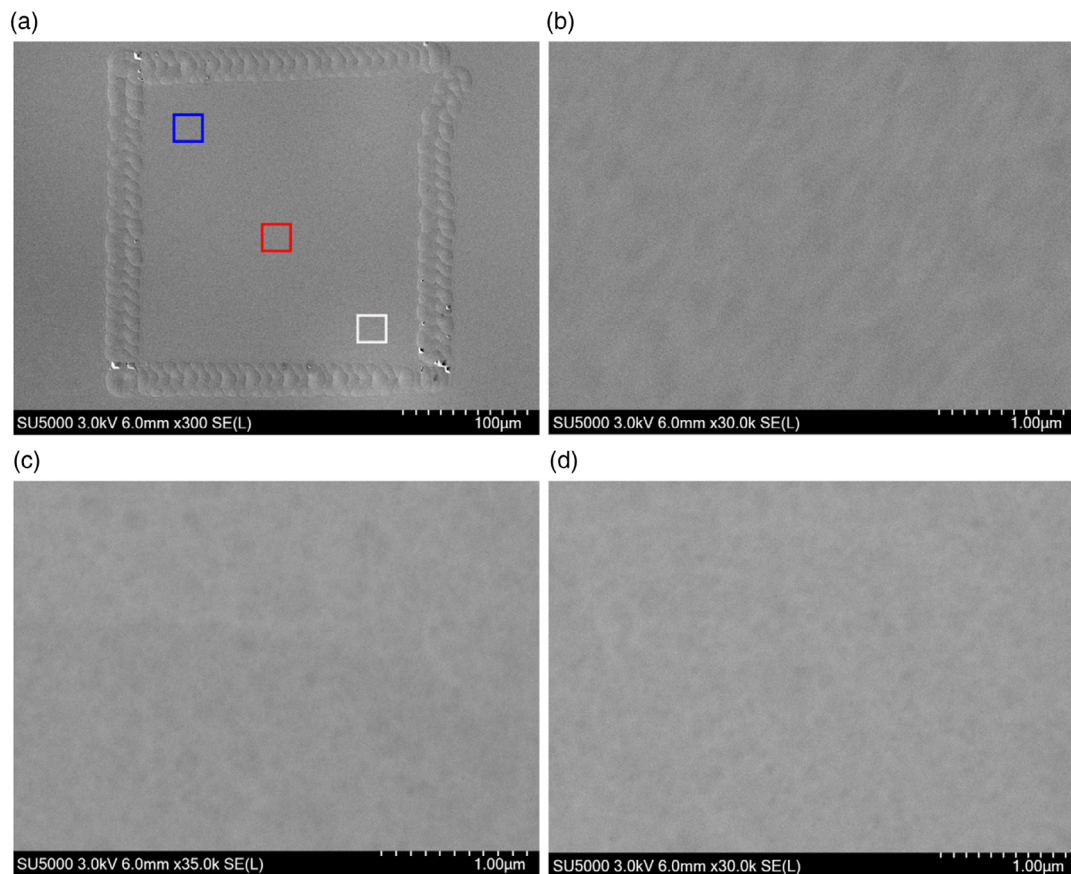


**Figure 4.** a) SEM image of one of the laser-marked squares processed using methodology as reported in our previous work<sup>[14]</sup> for the investigation of the pinholes in DI- $\text{O}_3$  oxide layer. b–d) The magnified view of the white, red, and blue squares drawn in (a).



Thereafter, the quality of the DI-O<sub>3</sub> oxide processed by improved SD was further accessed by investigating pinholes therein. Samples were prepared using a four-step methodology as discussed in ref. [14]. Briefly, the sample was first laser marked in square shapes of sizes 250 × 250 μm on six different locations on the wafer. Then, the wafer was etched in 25 aq. wt% TMAH solution to remove any splatters and saw damage. The wafer was then cleaned in DI-O<sub>3</sub> bath, followed by the growth of a fresh DI-O<sub>3</sub> oxide. Thereafter, the wafer was again etched in TMAH followed by HF etch, DI water rinse, and improved SD for drying. Then the SEM imaging was performed. **Figure 4a** shows that pinholes/etch marks are visible only at the laser-marked line and are absent inside the square under discussion that confirms grown DI-O<sub>3</sub> oxide, dried using improved SD, are pinholes free. To support the argument, further SEM imaging at higher magnification was carried out at three different locations within the laser-marked square as shown by different colored regions in **Figure 4a**. The colored drawn regions, i.e., white, red, and blue in **Figure 4a** are shown separately in **Figure 4b–d** wherein we could not observe any pinholes.

### 3. Conclusion

In summary, we investigated two methods, i.e., SD and ND, for drying wafers grown with the ultrathin oxide through the wet chemical process, i.e., ozone-dissolved DI water. Experiments showed that although SD method provides the good oxide uniformity (around ±4.17%) across 100 mm diameter wafer, DI-O<sub>3</sub> oxide samples processed by ND were consistently resulted with poor uniformity (±21.67%). However, the results of DI-O<sub>3</sub> oxide samples processed by SD, then passivated with AlO<sub>x</sub>, were repeatedly associated with inferior performance than that by ND. It is found that drying DI-O<sub>3</sub> oxide samples with SD as a last step is the prime cause of persistently poor passivation quality. Findings of this work depict that drying wafers with SD as the last step generates static charges on the wafer surface that eventually degrades the passivation quality. An improved SD method is demonstrated, in which wafers are dried in SD first, then rinsed in DIW, and lastly with ND; this technique apparently neutralizes the detrimental static charges. The improved SD method, developed as part of this contribution, not only improves the passivation significantly, but also provides the highly uniformed oxide across the sample. The improved wafer spin-drying process developed in this work could be readily applied in other oxides grown by wet chemical processes. Lastly, we have demonstrated that DI-O<sub>3</sub> oxide samples processed by improved SD are also free of pinholes.

### 4. Experimental Section

N-type <100> 300 μm thick 100 mm diameter ≈5 Ω cm Cz DSP wafers were used in this contribution. 25 aq wt% tetramethylammonium hydroxide (TMAH) solution at a temperature of 90 °C was used for saw damage removal. Ultra-thin silicon oxide was grown in ozone-dissolved deionized water at a constant flow of 420 mL min<sup>-1</sup>, 15 ppm ozone concentration, and 25 °C of operating temperature. Thickness and uniformity of DI-O<sub>3</sub> oxide was measured by Film Sense Multi-Wavelength Ellipsometer System featuring 6 wavelengths: 405–950 nm spectral range, along with the motorized sample stage capable of mapping 150 mm diameter.

Semitoool STI 870 Spin Rinser Dryer Double Stack was used for spin-drying the wafers at 1000 rpm for 90 s.<sup>[38]</sup> During the SD process, the chamber was constantly filled with N<sub>2</sub> gas. The entire DI-O<sub>3</sub> growth process was carried out at room temperature and the process timings were already optimized in our previous work.<sup>[17]</sup> AlO<sub>x</sub> deposition using TMA and H<sub>2</sub>O took place in a thermal atomic layer deposition (ALD) system (Cambridge NanoTech Savannah 100 ALD) with a deposition rate of 0.088 nm per cycle at 200 °C. Transient photoconductance decay (PCD) technique enabled by Sinton WCT-120 was used to measure effective carrier lifetime,  $\tau_{\text{eff}}$  and saturation current density,  $J_0$  (per side) at excess carrier densities of  $1 \times 10^{15}$  and  $5 \times 10^{15}$  cm<sup>-3</sup>, respectively. To enhance  $J_0$  accuracy, measurements were taken at carrier injections significantly higher than  $\tau_{\text{eff}}$ , ensuring a clear distinction between surface and bulk effects. Symmetrically passivated samples were used for both  $\tau_{\text{eff}}$  and  $J_0$  measurements. Pinholes in the DI-O<sub>3</sub> oxide layers were analyzed using a Hitachi SU5000 field-emission scanning electron microscope (FE-SEM).

### Acknowledgements

The material was based upon work supported by the U.S. Department of Energy's Office of Energy Efficiency and Renewable Energy (EERE) under the Solar Energy Technologies Office Award Number DE-EE0009367.

### Conflict of Interest

The authors declare no conflict of interest.

### Author Contributions

**Vibhor Kumar**: investigation: (supporting); methodology: (supporting); writing—original draft: (equal); writing—review & editing: (supporting). **Munan Gao**: formal analysis: (equal); investigation: (equal); methodology: (equal); writing—original draft: (equal); writing—review & editing: (supporting). **Ngwe Zin**: conceptualization: (lead); formal analysis: (lead); funding acquisition: (lead); investigation: (lead); methodology: (lead); project administration: (lead); resources: (lead); supervision: (lead); writing—original draft: (lead); writing—review & editing: (lead).

### Data Availability Statement

The data that support the findings of this study are available from the corresponding author upon reasonable request.

### Keywords

carrier lifetime and saturation current density, dissolved ozone oxide DI-O<sub>3</sub>, field-effect passivation, spin-dry

Received: October 8, 2024  
Revised: November 9, 2024  
Published online: December 18, 2024

- [1] J. Zhao, A. Wang, M. A. Green, *Prog. Photovoltaics: Res. Appl.* **1999**, 7, 471.
- [2] R. S. Bonilla, I. Al-Dhahir, M. Yu, P. Hamer, P. P. Altermatt, *Sol. Energy Mater. Sol. Cells* **2020**, 215, 110649.
- [3] P. Stradins, S. Essig, W. Nemeth, B. G. Lee, D. Young, A. Norman, Y. Liu, J.-W. Luo, E. Warren, A. Dameron, V. LaSalvia, M. Page, presented at WCPEC-6: 6th World Conf. on Photovoltaic Energy Conversion,

- Kyoto, Japan, November 2014 <https://www.nrel.gov/docs/fy15osti/63259.pdf>.
- [4] S. W. Glunz, F. Feldmann, *Sol. Energy Mater. Sol. Cells* **2018**, 185, 260.
- [5] J. Schmidt, A. Merkle, R. Brendel, B. Hoex, M. C. M. v. de Sanden, W. M. M. Kessels, *Prog. Photovoltaics: Res. Appl.*, **2008**, 16, 461.
- [6] G. Dingemans, W. M. M. Kessels, *J. Vac. Sci. Technol. A* **2012**, 30, 040802.
- [7] S. Z. Y. Chen, M. Tan, W. Shen, *Front. Energy* **2017**, 11, 52.
- [8] J. Schmidt, R. Peibst, R. Brendel, *Sol. Energy Mater. Sol. Cells* **2018**, 187, 39.
- [9] N. Grant, K. R. McIntosh, in *48th AuSES Annual Conf.*, Australian Solar Energy Society, Australia **2010**, pp. 1–10, <https://doi.org/10.13140/2.1.3541.3443>.
- [10] N. E. Grant, K. R. McIntosh, *IEEE Electron. Dev. Lett.* **2009**, 30, 922.
- [11] T. K. Jayalakshmi, S. Shah, I. Lobo, A. Uppe, A. Mehta, *Lung India* **2009**, 26, 149.
- [12] M. Gao, V. Kumar, W. Schoenfeld, N. Zin, *IEEE J. Photovoltaics* **2023**, 13, 385.
- [13] Y. Wang, Z. Gu, L. Li, S. Liu, J. Li, L. Lu, X. Li, W. Liu, R. Liu, J. Chen, Y. Wang, S.-T. Zhang, D. Li, *Mater. Today Energy* **2023**, 35, 101336.
- [14] V. Kumar, M. Gao, N. Zin, *Phys. Status Solidi RRL* **2023**, 17, 2200325.
- [15] A. Moldovan, F. Feldmann, K. Kaufmann, S. Richter, M. Wemer, C. Hagendorf, M. Zimmer, I. Rentschl, M. Hermle, in *2015 IEEE 42nd Photovoltaic Specialist Conf. (PVSC)*, IEEE, Piscataway, NJ **2015**, pp. 1–6.
- [16] A. Fischer, A. Moldovan, J. Temmler, M. Zimmer, J. Rentsch, *AIP Conf. Proc.* **2018**, 1999, 050001.
- [17] M. Gao, V. Kumar, N. Zin, in *2022 IEEE 49th Photovoltaics Specialists Conf. (PVSC)*, IEEE, Piscataway, NJ **2022**, pp. 0620–0622.
- [18] V. K. M. Gao, N. Zin, in *IEEE 50th Photovoltaic Specialists Conf. (PVSC)*, IEEE, Piscataway, NJ **2023**.
- [19] F. D. Smedt, C. Vinckier, I. Cornelissen, S. D. Gendt, M. Heyns, *J. Electrochem. Soc.* **2000**, 147, 1124.
- [20] W. A. S. Glenn, W. Gale, J. A. Brigante, State-of-The-Art Drying Methods for Semiconductor Wet Benches, [https://www.electrochem.org/semiconductor\\_cleaning/pv\\_97\\_35.pdf](https://www.electrochem.org/semiconductor_cleaning/pv_97_35.pdf).
- [21] K. A. Reinhardt, R. F. Reidy, J. A. Marsella, in *Handbook for Cleaning for Semiconductor Manufacturing: Fundamentals and Applications*, Scrivener Publishing, Salem, MA **2011**.
- [22] H. W. Kim, *J. Mater. Sci.* **2004**, 39, 4669.
- [23] K. P. Roenker, *IEEE Trans. Electron. Dev.* **1984**, 31, 1838.
- [24] F. Oktasendra, R. Hidayat, R. I. Utama, *J. Phys.: Conf. Ser.* **2020**, 1481, 012005.
- [25] A. S. Kale, W. Nemeth, S. P. Harvey, M. Page, D. L. Young, S. Agarwal, P. Stradins, *Sol. Energy Mater. Sol. Cells* **2018**, 185, 270.
- [26] P. Saint-Cast, F. Tanay, M. Alemán Martínez, C. Reichel, J. Bartsch, M. Hofmann, J. Rentsch, R. Preu, *Relevant Pinhole Characterisation Methods for Dielectric Layers for Silicon Solar Cells* **2009**, pp. 2084–2087, <http://www.eupvsec-proceedings.com/proceedings?paper=4230> (accessed: July 2024)
- [27] D. Kray, S. Glunz, *Prog. Photovoltaics: Res. Appl.* **2006**, 14, 195.
- [28] F. Granek, M. Hermle, C. Reichel, O. Schultz-Wittmann, S. Glunz, in *23rd European Photovoltaic Solar Energy Conf., 1–5 September 2008, Valencia, Spain*, WIP-Renewable Energies, Munich **2008**, pp. 991–995.
- [29] S. Bakhshi, N. Zin, H. Ali, M. Wilson, D. Chanda, K. O. Davis, W. V. Schoenfeld, *Sol. Energy Mater. Sol. Cells* **2018**, 185, 505.
- [30] R. S. Bonilla, P. R. Wilshaw, *Appl. Phys. Lett.* **2014**, 104, 213108.
- [31] J. John, *IET Energy Engineering*, Vol. 106, The Institution of Engineering and Technology (IET), London, UK **2018**, p. Xxiii.
- [32] H. Inaba, S. Sakata, T. Yoshida, T. Okada, T. Ohmi, *IEEE Trans. Semicond. Manuf.* **1992**, 5, 234.
- [33] V. Murali, A. Wu, A. Chatterjee, D. Fraser, *IEEE Trans. Semicond. Manuf.* **1992**, 5, 214.
- [34] T. S. M. Wada, H. Takahashi, N. Hayashi, A. Eitoku, *Solid State Phenom.* **2007**, 134, 263.
- [35] V. Menon, B. DeSelms, J. Chacon, E. Kamieniecki, *Microcontamination* **1990**, 8, 23.
- [36] B. Hoex, J. Schmidt, P. Pohl, M. Van de Sanden, W. Kessels, *J. Appl. Phys.* **2008**, 104, 044903.
- [37] T. Ohmi, in *Ultra-Clean Technology Handbook: Volume 1: Ultra-Pure Water*, CRC Press, Boca Raton, FL **2017**.
- [38] R. E. N. J. Ruzyllo, C. Appel, T. Hattori, M. Heyns, in *Cleaning Technology in Semiconductor Device Manufacturing*, The Electrochemical Society, Inc., Pennington, NJ **1998**.